Large-scale inhomogeneity of dark energy produced in the ancestor vacuum

Yue Nan,[1] Kazuhiro Yamamoto,[1,2] Hajime Aoki,[3] Satoshi Iso,[4] and Daisuke Yamauchi[5]
[1]*Department of Physics, Graduate School of Science, Hiroshima University, Higashi-Hiroshima 739-8526, Japan*
[2]*Department of Physics, Kyushu University, 744 Motooka, Nishi-Ku, Fukuoka 819-0395, Japan*
[3]*Department of Physics, Saga University, Saga 840-8502, Japan*
[4]*Theory Center, High Energy Accelerator Research Organization (KEK), and Graduate University for Advanced Studies (SOKENDAI), Ibaraki 305-0801, Japan*
[5]*Faculty of Engineering, Kanagawa University, Kanagawa 221-8686, Japan*

(Received 4 February 2019; published 10 May 2019)

We investigate large-scale inhomogeneity of dark energy in the bubble nucleation scenario of the universe. In this scenario, the present universe was created by a bubble nucleation due to quantum tunneling from a metastable ancestor vacuum, followed by a primordial inflationary era. During the bubble nucleation, supercurvature modes of some kind of a scalar field are produced, and remain until present without decaying; thus they can play a role of the dark energy, if the mass of the scalar field is sufficiently light in the present universe. The supercurvature modes fluctuate at a very large spatial scale, much longer than the Hubble length in the present universe. Thus they create large-scale inhomogeneities of the dark energy, and generate large-scale anisotropies in the cosmic microwave background (CMB) fluctuations. This is a notable feature of this scenario, where quantum fluctuations of a scalar field are responsible for the dark energy. In this paper, we calculate imprints of the scenario on the CMB anisotropies through the integrated Sachs-Wolfe (ISW) effect, and give observational constraints on the curvature parameter Ω_K and on an additional parameter ϵ describing some properties of the ancestor vacuum.

DOI: 10.1103/PhysRevD.99.103512

I. INTRODUCTION

The standard cosmological model, the ΛCDM model, describes the history of our universe which is composed of radiation, baryonic matter, cold dark matter (CDM) and dark energy represented by the cosmological constant Λ. Observations of the large-scale structures have played important roles in determining the fraction of each component to the total energy density: approximately 30% for the matter components and 70% for the dark energy. Another possible ingredient, the spatial curvature of the universe Ω_K, is known to be very close to zero, and our universe is almost spatially flat [1–4]. The ΛCDM model, together with the assumption of the primordial inflation, has successfully explained various cosmological observations: e.g., the cosmic microwave background (CMB) anisotropies, the abundance of light elements in the early universe, the baryonic acoustic oscillation (BAO) peaks, and the formation of the cosmological structures.

Dark energy is the most dominant component of the present universe, and accelerates the expansion of the universe [5]. But its nature is unknown and the origin of the dark energy is the most intriguing riddle in the universe. The simplest hypothesis for dark energy is the cosmological constant Λ, which has survived various observational tests, by e.g., the Planck satellite, the Baryon Oscillation Spectroscopic Survey (BOSS) in the Sloan Digital Sky Survey (SDSS) project, and the Dark Energy Survey (DES). On the other hand, it is recently argued that the cosmological constant cannot be compatible with string theory predictions [6–9]. Indeed, many dynamical scenarios for the dark energy predict different equations of state (EoS), $w \neq -1$, which can be tested or falsified by observations [10–12]. An example is the quintessence model based on a classically rolling scalar field [13]. Other examples are based on quantum fluctuations of ultralight scalar fields (e.g., [14–20]). In this context, a connection with the string axiverse scenario is interesting [21–23].

In the present paper, we investigate one of such dynamical scenarios of the dark energy [24,25]. It is based on a bubble nucleation of our universe from a metastable *ancestor* vacuum in de Sitter spacetime. The universe is assumed to be created by quantum tunneling of a scalar field, which is semiclassically described by the Coleman-De Luccia (CDL) instanton [26]. We note that bubble-nucleation transitions could be a characteristic feature of the string landscape scenario [27–30]. Following the scenario, the present universe is then described by an open Friedmann-Lemaitre-Robertson-Walker (FLRW) universe with negative spatial curvature. In addition, we introduce a scalar field ϕ, which is different from the CDL tunneling field. Then the tunneling from the ancestor vacuum

generates very long wavelength modes of the ϕ field; the supercurvature modes. These modes remain out of the horizon until present and can play a role of the dark energy in the present epoch.

The supercurvature modes are the so-called discrete modes and have an imaginary wave number on the three-dimensional sphere S_3 in the Euclidean CDL geometry. Because of this, the modes are non-normalizable on the hyperbolic H_3, when they are analytically continued from the Euclidean CDL geometry to the Lorentzian region to describe a bubble nucleation in de Sitter spacetime [31–33]. As long as the mass of the scalar field is sufficiently light, the supercurvature modes decay slowly at large distances, and give rise to long-range fluctuations of the field in the open universe. The length scale of the fluctuations, which is called the supercurvature scale $L_{\rm sc}$, is much larger than the present spatial curvature scale L_c of the Universe and the Hubble length H_0^{-1} at present; $L_{\rm sc} \gg L_c \gtrsim 10H_0^{-1}$. Thus, the supercurvature-mode energy density takes an almost constant value within the horizon scale of the observable universe; it behaves as the dark energy, and we call it the supercurvature-mode dark energy. Possible observable signatures of the scenario in the EoS have been investigated in Ref. [25] with an expectation of being verified in the galaxy surveys by Square Kilometre Array (SKA) and Euclid mission in the forthcoming decade [34]. In the present paper, we further investigate another verifiable property of the supercurvature-mode dark energy. A novel feature of the supercurvature-mode dark energy is that the mode is not exactly homogeneous and may induce tiny anisotropies and inhomogeneities of the dark energy even on the scale of the observable universe (cf. [35]). The anisotropies are transformed into the anisotropic patterns of the CMB spectrum through the late-time integrated Sachs-Wolfe (ISW) effect, which can distinguish the model from the simplest ΛCDM model.

The paper is organized as follows. In Sec. II, we will review the setup of the supercurvature-mode dark energy scenario and calculate the spatial correlation of the dark energy density contrast. In Sec. III, we calculate the two-point correlation function of the CMB fluctuations. The inhomogeneity of the supercurvature-mode dark energy is imprinted in the large-angle correlation of the CMB anisotropies. Comparison with the observational data put upper bounds on the curvature parameter Ω_K and the parameter ϵ that describes some properties of the ancestor vacuum. Finally, in Sec. IV, we will summarize the results. Details of calculations are given in Appendices.

II. SPATIAL CORRELATION OF THE SUPERCURVATURE-MODE DARK ENERGY

In this section, we first briefly review the supercurvature-mode dark energy scenario following [24,25]. In this model, the dark energy behaves nearly identical to the cosmological constant except for spatial inhomogeneities on very large scales. Then, we calculate spatial variations of the dark energy, which motivates the investigations of detectability through the CMB anisotropies in the next section. Suppose that our universe is an open universe created by a bubble nucleation due to the CDL quantum tunneling of a scalar field [26]. After the bubble nucleation, the primordial inflation occurred first and then the big bang universe with negative spatial curvature has started. We also introduce another scalar field ϕ whose supercurvature mode is generated through the bubble nucleation process. The mode will become the dark energy, which we call the supercurvature-mode dark energy. Before the tunneling, in the metastable de Sitter (ancestor) vacuum, Hubble parameter and mass of ϕ are denoted by H_A and m_A, respectively. Ordinary inflation follows the bubble nucleation in the hyperbolic spatial geometry. The Hubble parameter of the inflation is denoted by H_I. We note that the Hubble parameters before and after the CDL quantum tunneling satisfy the relation $H_A > H_I$ [24]. The mass of the scalar field ϕ after the tunneling is set m_0, which could be different from m_A.

In the free field approximation, we can solve the equation of motion for the scalar field ϕ on the CDL background in Euclidean space; expanding solutions in terms of the eigenfunctions on the 3-dimensional sphere slice S^3 with eigenvalues $-(k^2+1)$, the equation of motion becomes a Schrödinger-like equation with a finite potential. The eigenfunctions on S^3 are classified into two types of modes. One type is a continuous mode with a real wave number k while the other is a discrete mode with an imaginary wave number $k = i(1-\epsilon)$. The discrete mode is called the supercurvature mode. Here ϵ is determined by the properties of the ancestor vacuum and given by

$$\epsilon = c_\epsilon \left(\frac{m_A}{H_A}\right)^2, \tag{1}$$

where c_ϵ is an order $\mathcal{O}(1)$ quantity that depends on the critical size of the bubble created in the ancestor vacuum. The mass m_A of the scalar field and the Hubble parameter H_A in the ancestor vacuum are assumed to obey the condition $m_A \ll H_A$; thus $\epsilon \ll 1$ follows. Analytically continued to the Lorentzian region in de Sitter space, the supercurvature mode becomes non-normalizable on the spatial slicing H^3 of the open universe and generate large-scale fluctuations. Unlike the continuous modes that decay as $e^{-\eta}$ in the conformal time η, the discrete supercurvature mode behaves $e^{-\epsilon\eta}$ and decay remarkably slowly compared with the continuous modes. The scalar field is assumed to have ultralight mass $m_0 < H_0 \sim 10^{-33}$ eV, and the supercurvature mode plays a role of the dark energy in the present universe. A candidate of such ultralight fields may appear as an axionlike particle (ALP) in string theory [21,22].

In the following, we focus on the supercurvature modes and investigate its properties as the dark energy in the

present universe. The supercurvature mode contributes to the correlation function of the scalar field $\phi(x)$ in the open universe within the bubble as [24]

$$\langle\phi(\eta,\boldsymbol{x})\phi(\eta',\boldsymbol{x}')\rangle = \varphi(\eta)\varphi(\eta')\frac{\sinh(1-\epsilon)R}{(1-\epsilon)\sinh R}, \quad (2)$$

where η is the conformal time, $\varphi(\eta)$ is the frozen expectation value of field ϕ. The explicit form of φ is given in Eq. (A3). R is the (dimensionless) geodesic distance on the three-dimensional hyperbolic space H^3, normalized in terms of the curvature scale $L_c = 1/\sqrt{-K}$, and is given by

$$\cosh R = \cosh R_1 \cosh R_2 - \sinh R_1 \sinh R_2 \cos\psi. \quad (3)$$

R_1 and R_2 are the radial coordinates of the two points, $\boldsymbol{x}$ and $\boldsymbol{x}'$, and ψ is the included angle between them in the three-dimensional space (see Fig. 1). In the next section, we also use χ to denote the comoving radial coordinate distance with dimension of the length; $R = \sqrt{-K}\chi$. Thus the curvature radius is given by $R_c = \sqrt{-K}L_c = 1$.

Now we calculate the spatial variation of the supercurvature mode dark energy. In this model, the dark energy density at late times in the matter-dominated era (i.e., in the period (ii) in Sec. V C of Ref. [24]) is dominantly given by the mass term in the energy-momentum tensor of the supercurvature mode[1],

$$\rho_{\rm DE}(\eta,\boldsymbol{x}) \simeq \frac{m_0^2}{2}\phi^2(\eta,\boldsymbol{x}). \quad (4)$$

Then defining the density contrast of the dark energy by

$$\delta(\eta,\boldsymbol{x}) = \frac{\rho_{\rm DE}(\eta,\boldsymbol{x}) - \langle\rho_{\rm DE}(\eta,\boldsymbol{x})\rangle}{\langle\rho_{\rm DE}(\eta,\boldsymbol{x})\rangle} \simeq \frac{\phi^2(\eta,\boldsymbol{x}) - \langle\phi^2(\eta,\boldsymbol{x})\rangle}{\langle\phi^2(\eta,\boldsymbol{x})\rangle}, \quad (5)$$

two point function of the density contrast can be calculated as

$$\langle\delta(\eta,\boldsymbol{x})\delta(\eta,\boldsymbol{y})\rangle = \frac{\langle\phi^2(\eta,\boldsymbol{x})\phi^2(\eta,\boldsymbol{y})\rangle - \langle\phi^2(\eta,\boldsymbol{x})\rangle\langle\phi^2(\eta,\boldsymbol{y})\rangle}{\langle\phi^2(\eta,\boldsymbol{x})\rangle^2}, \quad (6)$$

[1]At earlier times (i.e., in the period (i) in Sec. V C of Ref. [24]), the spatial-derivative term dominates over the mass term and the EoS parameter w approaches $-1/3$. Possible observational signatures of the time-dependent EoS are investigated in Ref. [25]. However, for the analyses of the large-scale inhomogeneity that will be studied in the present paper, this effect only gives higher order corrections, and we will ignore it. See Appendix B.

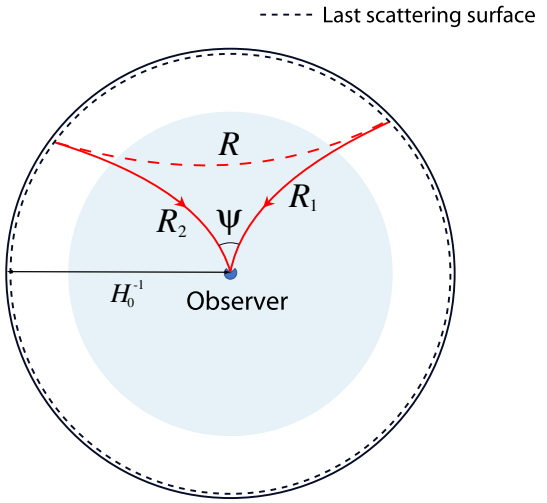

FIG. 1. Schematic of the choice of $\{R, R_1, R_2\}$ triplets along different line-of-sight for the two-point correlation function.

where we used $\langle\phi^2(\eta,\boldsymbol{x})\rangle = \langle\phi^2(\eta,\boldsymbol{y})\rangle$. Furthermore, in the free field approximation, we can decompose the four-point function of ϕ into a product of two-point functions by using the Wick theorem:

$$\langle\phi^2(\eta,\boldsymbol{x})\phi^2(\eta,\boldsymbol{y})\rangle = \langle\phi^2(\eta,\boldsymbol{x})\rangle\langle\phi^2(\eta,\boldsymbol{y})\rangle + 2\langle\phi(\eta,\boldsymbol{x})\phi(\eta,\boldsymbol{y})\rangle^2. \quad (7)$$

Then, using Eq. (2), we have

$$\xi(R) \equiv \langle\delta(\eta,\boldsymbol{x})\delta(\eta,\boldsymbol{y})\rangle = \frac{2\langle\phi(\eta,\boldsymbol{x})\phi(\eta,\boldsymbol{y})\rangle^2}{\langle\phi^2(\eta,\boldsymbol{x})\rangle^2} = 2\left(\frac{\sinh(1-\epsilon)R}{(1-\epsilon)\sinh R}\right)^2, \quad (8)$$

where $R = \sqrt{-K}|\boldsymbol{x}-\boldsymbol{y}|$. The correlation function $\xi(R)$ changes its behavior around the curvature scale $R_c = 1$ as

$$\xi(R) \simeq 2 \times \begin{cases} 1 & R \ll 1 \\ e^{-2\epsilon R} & R \gg 1 \end{cases}, \quad (9)$$

and diminishes at distances over the supercurvature scale $R_{\rm sc} \equiv 1/\epsilon$. In physical length, $R_{\rm sc}$ corresponds to $L_{\rm sc} = L_c/\epsilon$, which is much larger than the curvature radius L_c. The behavior of $\sqrt{\xi(R)}$ for $R \gg R_{\rm sc}$ is depicted in Fig. 2. This indicates that the supercurvature-mode dark energy density varies considerably beyond the supercurvature scale $R_{\rm sc}$. In Fig. 3, we show a schematic picture of the spatial variation of the supercurvature-mode dark energy. At the horizon scale $H_0^{-1}(\ll L_c)$, we take $R = \sqrt{-K}H_0^{-1} = \sqrt{\Omega_K}$, where we used the relation $\Omega_K = -K/H_0^2$. For Ω_K, $\epsilon \ll 1$, we have

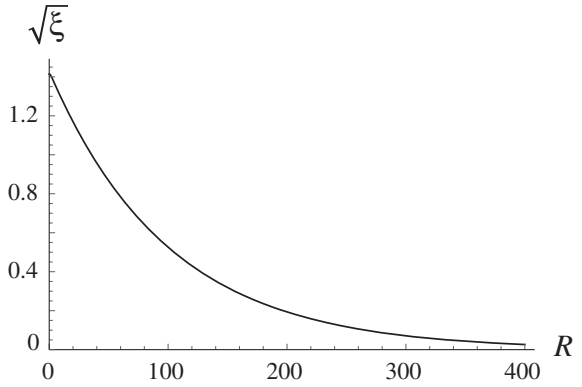

FIG. 2. $\xi^{1/2}(R)$ as a function of R, where we adopted $\epsilon = 0.01$. The horizon scale at the present epoch is $R \sim \sqrt{-K}/H_0 = \sqrt{\Omega_K} \ll 1$, the curvature scale is $R = 1$, and the supercurvature scale is $R = 1/\epsilon \gg 1$.

$$\sqrt{\langle\delta^2(0)\rangle} - \sqrt{\langle\delta(0)\delta(1/H_0)\rangle} = \sqrt{2} - \sqrt{2}\frac{\sinh(1-\epsilon)\sqrt{\Omega_K}}{(1-\epsilon)\sinh\sqrt{\Omega_K}} \simeq \sqrt{2}\frac{\epsilon\Omega_K}{3}, \quad (10)$$

which is extremely tiny ($\propto\epsilon\Omega_K$). However, as we will see in the next section, it may give rise to an observable effect in the CMB anisotropies on the large scales.

The above results show that the density contrast of the supercurvature-mode dark energy has an inhomogeneity of the order one over the scales of the supercurvature $R \gtrsim R_{\rm sc} \gg 1$. This large-scale variation of the dark energy density is the characteristic feature of the dark energy model based on quantum fluctuations. For the large scales

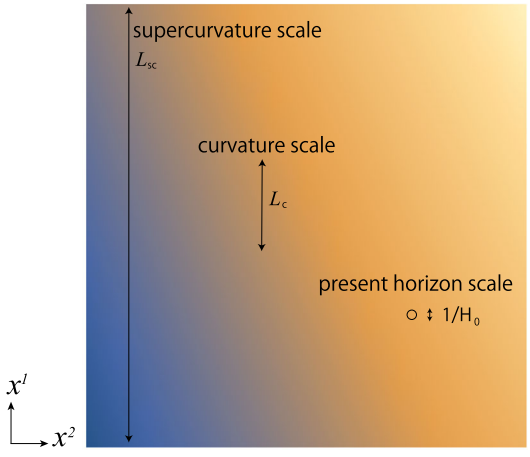

FIG. 3. Schematic for supercurvature-mode dark energy density contrast, where the brightness of the color denotes the relative amplitude of the density contrast. We assume that the supercurvature scale $L_{\rm sc} = 1/\epsilon\sqrt{-K}(= L_c/\epsilon)$ is far beyond the curvature scale $L_c = 1/\sqrt{-K}$. The curvature scale L_c is beyond the comoving horizon scale so that the observable universe appears flat. The horizon scale at the present epoch is $1/H_0$. Thus, we assume $1/H_0 \ll L_c \ll L_{\rm sc}$.

$R > R_{\rm sc}$, the dark energy density largely fluctuates and can be treated as a classical Gaussian random variable with the properties of $\langle\phi_{\rm sc}\rangle = 0$ and $\langle\phi_{\rm sc}^2\rangle = \varphi^2(\eta)$ [See Appendix A for the explicit expression of $\varphi(\eta)$]. On the other hand, the dark energy density is nearly constant within the horizon $H_0^{-1}(\ll L_c)$. The explicit form of the probability distribution function of the dark energy density is shown in Appendix C. The result demonstrates a wide distribution of probability of $\rho_{\rm DE}$ and the dark energy density parameter Ω_Λ at scales larger than the supercurvature scale $R_{\rm sc}$ even when we fix the parameter

$$\langle\rho_{\rm DE}(\boldsymbol{x})\rangle = \frac{1}{2}m_0^2\varphi^2(0) = 3H_0^2\bar{\Omega}_\Lambda/8\pi G \quad (11)$$

with $\bar{\Omega}_\Lambda = 0.7$. Thus the dark energy density has a large spatial variation on the large scales $R > R_{\rm sc}$. We also note that even within the horizon scale, H_0^{-1}, there exists the spatial variation, though it is tiny as Eq. (10). In the next section, we will study the CMB anisotropies caused by it, and give observational constraints on the model parameters of the scenario.

III. CMB ANISOTROPIES FROM THE SUPERCURVATURE-MODE

To study observable effects from the spatial variations of the supercurvature-mode dark energy, we investigate possible imprints from the supercurvature-mode dark energy on the CMB anisotropies through the late-time ISW effect. We adopt the line element under the conformal Newtonian gauge as

$$ds^2 = a^2(\eta)[-(1+2\Psi)d\eta^2 + (1+2\Phi)\gamma_{ij}dx^i dx^j], \quad (12)$$

where Ψ and Φ are the gravitational potential and the curvature potential, respectively, and γ_{ij} is the three-dimensional metric in an open universe,

$$\gamma_{ij}dx^i dx^j = d\chi^2 + \left(\frac{\sinh\sqrt{-K}\chi}{\sqrt{-K}}\right)^2(d\theta^2 + \sin^2\theta d\varphi^2). \quad (13)$$

The evolution of the distribution function of CMB photons is described by the Boltzmann equation with the perturbed Planck distribution:

$$f(\eta,\boldsymbol{x},\boldsymbol{p}) = \frac{1}{\exp[p/(T(\eta)(1+\Theta(\eta,\boldsymbol{x},\boldsymbol{\gamma}))] - 1}, \quad (14)$$

where $\Theta(\eta,\boldsymbol{x},\boldsymbol{\gamma})$ denotes the temperature fluctuation of photons. $\boldsymbol{\gamma}$ is the line-of-sight direction identical to the unit vector of the observed photon momentum $\boldsymbol{p}$, while p is its magnitude. Note that the temperature fluctuation $\Theta(\eta,\boldsymbol{x},\boldsymbol{\gamma})$ depends on the photon's trajectory scattered from the past. It can be shown that the CMB anisotropy $\Theta(\eta,\boldsymbol{x},\boldsymbol{\gamma})$ satisfies the equation [36]

$$\frac{d}{d\eta}(\Theta+\Psi)=\frac{\partial\Psi(\eta,\boldsymbol{x})}{\partial\eta}-\frac{\partial\Phi(\eta,\boldsymbol{x})}{\partial\eta}+C_{e\gamma}, \quad (15)$$

where $C_{e\gamma}$ denotes the collision term for the Compton scattering, but it can be omitted in our investigation. Then, the integration yields the ISW contribution to the CMB anisotropies,

$$\frac{\Delta T}{T}(\boldsymbol{\gamma})=\Theta(\eta_0,\boldsymbol{x}_0,\boldsymbol{\gamma})+\Psi(\eta_0,\boldsymbol{x}_0)=\int_{\eta_*}^{\eta_0}d\eta\left(\frac{\partial\Psi(\eta,\chi,\boldsymbol{\gamma})}{\partial\eta}-\frac{\partial\Phi(\eta,\chi,\boldsymbol{\gamma})}{\partial\eta}\right)\Big|_{\chi=\eta_0-\eta}. \quad (16)$$

Here, on the right-hand side, the spatial position $\boldsymbol{x}$ is represented by its radial coordinate and the angle as $\boldsymbol{x}=(\chi,\boldsymbol{\gamma})$. The direction of the photon, $\boldsymbol{\gamma}$, is fixed in this expression and the radial coordinate $\chi=\eta_0-\eta$ denotes the position of the photon at the conformal time η. η_* stands for the conformal time of the CMB last scattering surface. Hereafter, we use *dot* to denote a differentiation with respect to the conformal time η, $\dot{}\equiv\partial/\partial\eta$. In the following, we calculate the right-hand-side of Eq. (16) by using the perturbed Einstein equation.

Using an overbar to represent the background quantity, we have the 0th order Einstein equation [36],

$$\bar{G}^0{}_0=-3\frac{1}{a^2}(\mathcal{H}^2+K)=8\pi G\bar{T}^0{}_0=8\pi G(\bar{T}^0{}_{0(\mathrm{m})}+\bar{T}^0{}_{0(\phi)}), \quad (17)$$

where (m) and (ϕ) denotes the matter component and the dark energy component, respectively, and we defined $\mathcal{H}=\dot{a}/a=a_{,\eta}/a$. A definition of the overbar will be shown momentarily. The 1st order perturbation of the Einstein equation is given by

$$\delta G^0{}_0=2\frac{1}{a^2}[3\mathcal{H}^2\Psi-3\mathcal{H}\dot{\Phi}+(\nabla_H^2+3K)\Phi]=8\pi G\delta T^0{}_0=8\pi G(\delta T^0{}_{0(\mathrm{m})}+\delta T^0{}_{0(\phi)}), \quad (18)$$

where ∇_H^2 is the Laplacian defined with respect to γ_{ij} as $\nabla_H^2Q=\gamma^{ij}Q_{|ij}$ (See e.g., Ref. [36]).

On the other hand, the energy-momentum tensor for the scalar field ϕ is given by

$$T^0{}_{0(\phi)}=-\frac{1}{2a^2}((1-2\Psi)\dot{\phi}^2+(1-2\Phi)\gamma^{ij}\nabla_i\phi\nabla_j\phi+m_0^2a^2\phi^2). \quad (19)$$

Its spatial average surrounding our horizon is defined as

$$\bar{T}^0{}_{0(\phi)}=-\frac{1}{2a^2}((1-2\Psi)\dot{\phi}^2+(1-2\Phi)\gamma^{ij}\nabla_i\phi\nabla_j\phi+m_0^2a^2\phi^2)|_{\mathrm{SA}\chi=0}, \quad (20)$$

where "SA" denotes "spatially average around" surrounding the present Hubble scale of our Universe. We then consider the fluctuation of $T^0{}_{0(\phi)}$ around $\bar{T}^0{}_{0(\phi)}$,

$$\delta T^0{}_{0(\phi)}\equiv T^0{}_{0(\phi)}-\bar{T}^0{}_{0(\phi)}. \quad (21)$$

Since we are interested in the supercurvature-mode dark energy which is almost constant within the Hubble scale, we approximate the spatially averaged value by the quantity at the observer $\chi=0$. For example, we have

$$\phi(\eta,\chi,\boldsymbol{\gamma})|_{\mathrm{SA}\chi=0}=\phi(\eta,\chi=0,\boldsymbol{\gamma}). \quad (22)$$

Of course, $\phi(\eta,\chi=0,\boldsymbol{\gamma})$ does not depend on the direction $\boldsymbol{\gamma}$ and we can simply write it as $\phi(\eta,\chi=0)$. As we are interested in the dark energy component that fluctuates mildly both in space and time, the mass term in the energy-momentum tensor (19) dominantly contributes: $T^0{}_{0(\phi)}\simeq-\frac{1}{2}m_0^2\phi^2$. Then the background and the spatial fluctuation of $T^0{}_0$ are given by

$$\bar{T}^0{}_{0(\phi)}=-\frac{1}{2}m_0^2\phi^2|_{\mathrm{SA}\chi=0},\qquad \delta T^0{}_{0(\phi)}=-\frac{1}{2}m_0^2(\phi^2-\phi^2|_{\mathrm{SA}\chi=0}), \quad (23)$$

respectively.

Now let us calculate the temperature fluctuation induced by the autocorrelation of the supercurvature-mode dark energy. Since we are interested in the perturbations on the supercurvature scales, see Fig. 3, the metric perturbation in the late-time universe can be approximated as $\Psi+\Phi=0$ and the term $(\nabla_H^2+3K)\Phi$ is negligibly small. This allows us to approximate Eq. (18) as

$$\delta G^0{}_0=2\frac{1}{a^2}[3\mathcal{H}^2\Psi+3\mathcal{H}\dot{\Psi}]=8\pi G(\delta T^0{}_{0(\phi)}+\delta T^0{}_{0(\mathrm{m})}). \quad (24)$$

The perturbed energy momentum tensor of the matter component is $\delta T^0{}_{0(\mathrm{m})}=-\delta_{\mathrm{m}}\rho_{\mathrm{m}}$, where δ_{m} is the density contrast of the matter component, which follows (e.g., [36])

$$\dot{\delta}_{\mathrm{m}}+kV_{\mathrm{m}}+3\dot{\Phi}=0, \quad (25)$$

$$\dot{V}_{\mathrm{m}}+\frac{\dot{a}}{a}V_{\mathrm{m}}-k\Psi=0. \quad (26)$$

Here we follow the notation of Ref. [36] for the Fourier expansion in an open universe. Therefore, it should be understood that $k^2=-K(2\epsilon-\epsilon^2)$ for the supercurvature mode. These equations yield

$$(a\dot{\delta}_{\mathrm{m}})^{\cdot}+k^2a\Psi+3(a\dot{\Phi})^{\cdot}=0, \quad (27)$$

where we may omit the term of the gravitational potential $k^2a\Psi$, in the limit of the large scales, as we consider the supercurvature mode. Then, we have

$$\delta_{\rm m}(\eta) + 3\Phi(\eta) = 0, \tag{28}$$

where we assumed $\delta_{\rm m}(0) = \Phi(0) = 0$ for the super-curvature mode perturbations. With $\Psi + \Phi = 0$, Eq. (24) reduces to

$$6\frac{\mathcal{H}}{a^2}\dot{\Psi} + \left(6\frac{\mathcal{H}^2}{a^2} + 24\pi G\rho_m\right)\Psi = 8\pi G\delta T^0{}_{0(\phi)}. \tag{29}$$

Using Eqs. (23) and (29), we can write down the solution for Ψ as

$$\begin{aligned}\Psi(\eta,\chi,\boldsymbol{\gamma}) &= \frac{1}{F(\eta)}\int_{\eta_*}^{\eta} d\eta_1 \frac{8\pi G F(\eta_1)}{B(\eta_1)}\delta T^0{}_{0(\phi)}(\eta_1,\chi,\boldsymbol{\gamma}) \\ &\simeq -\frac{1}{F(\eta)}\int_0^{\eta} d\eta_1 \frac{4\pi G F(\eta_1)}{B(\eta_1)} \\ &\quad \times m_0^2(\phi(\eta_1,\chi,\boldsymbol{\gamma})^2 - \phi(\eta_1,0)^2),\end{aligned} \tag{30}$$

where the approximation $\eta_*/\eta \ll 1$, hence $\eta_* \simeq 0$ was used, and we defined

$$F(\eta) = F_c \exp\left\{\int_0^{\eta} d\eta' \frac{A(\eta')}{B(\eta')}\right\}, \tag{31}$$

$$A(\eta) = 6\frac{\mathcal{H}^2}{a^2} + 24\pi G\rho_m, \qquad B(\eta) = 6\frac{\mathcal{H}}{a^2}, \tag{32}$$

with a constant F_c. We note that the result of Eq. (30) does not depend on the constant F_c. Under the condition $\Phi + \Psi = 0$, Eq. (16) becomes

$$\frac{\Delta T}{T}(\boldsymbol{\gamma}) \simeq 2\int_0^{\eta_0} d\eta \left(\frac{\partial\Psi(\eta,\chi,\boldsymbol{\gamma})}{\partial\eta}\right)\Big|_{\chi=\eta_0-\eta}. \tag{33}$$

Thus using Eq. (30), the two-point correlation function of temperature fluctuations from the last scattering surface of the CMB is given by

$$\begin{aligned}\left\langle \frac{\Delta T}{T}(\boldsymbol{\gamma})\frac{\Delta T}{T}(\boldsymbol{\gamma}')\right\rangle &= 4\int_0^{\eta_0} d\eta_1 \int_0^{\eta_0} d\eta_2 \left[\frac{\partial}{\partial\eta_1}\frac{1}{F(\eta_1)}\int_0^{\eta_1} d\eta_3 \frac{4\pi G F(\eta_3)}{B(\eta_3)} m_0^2\right]\left[\frac{\partial}{\partial\eta_2}\frac{1}{F(\eta_2)}\int_0^{\eta_2} d\eta_4 \frac{4\pi G F(\eta_4)}{B(\eta_4)} m_0^2\right] \\ &\quad \times \langle(\phi(\eta_3,\chi_3,\boldsymbol{\gamma})^2 - \phi(\eta_3,0)^2)(\phi(\eta_4,\chi_4,\boldsymbol{\gamma}')^2 - \phi(\eta_4,0)^2)\rangle|_{\chi_3=\eta_0-\eta_1,\chi_4=\eta_0-\eta_2}.\end{aligned} \tag{34}$$

The expectation value in (34) can be decomposed into products of two-point functions by using the Wick-theorem in Eq. (7) and calculated by using the two-point correlation function in Eq. (2). The details of the calculation are given in Appendix D, and we obtain

$$\begin{aligned}\left\langle \frac{\Delta T}{T}(\boldsymbol{\gamma})\frac{\Delta T}{T}(\boldsymbol{\gamma}')\right\rangle &= \int_0^1 da_1 \int_0^1 da_2 \left[\frac{\partial}{\partial a_1}\frac{1}{F(a_1)}\int_0^{a_1} da_3 \frac{4\pi G m_0^2 F(a_3)}{3a_3 H^2(a_3)}\right]\left[\frac{\partial}{\partial a_2}\frac{1}{F(a_2)}\int_0^{a_2} da_4 \frac{4\pi G m_0^2 F(a_4)}{3a_4 H^2(a_4)}\right] \\ &\quad \times (-4)\varphi^2(\eta_3)\varphi^2(\eta_4)\epsilon\left[-\frac{2}{3}R_1R_2\cos\psi - \frac{2}{15}R_1^2R_2^2\left(\frac{3}{2}\cos^2\psi - \frac{1}{2}\right)\right],\end{aligned} \tag{35}$$

where $R_1 = \sqrt{-K}(\eta_0 - \eta_1)$ and $R_2 = \sqrt{-K}(\eta_0 - \eta_2)$, and η_i are functions of a_i as $\eta_i \equiv \eta(a_i)$ with $i = 1, 2, 3, 4$ respectively, whose explicit form is given in Appendix E, while $H(a)$ is the Hubble parameter.

In the rest of the paper, we will compare the result of Eq. (35) with the CMB observations and constraint on the model parameters in the present scenario. The multipole expansion of the angular two-point function of the CMB temperature fluctuation is expressed as

$$\left\langle \frac{\Delta T}{T}(\boldsymbol{\gamma})\frac{\Delta T}{T}(\boldsymbol{\gamma}')\right\rangle = \frac{1}{4\pi}\sum_{\ell}(2\ell+1)C_\ell P_\ell(\cos\psi), \tag{36}$$

where $\cos\psi = \boldsymbol{\gamma}\cdot\boldsymbol{\gamma}'$. Then, by comparing Eqs. (35) and (36), it is explicit to find

$$\frac{3}{4\pi}C_1 = S_1^2\frac{8}{3}\epsilon \sim \mathcal{O}(\epsilon\Omega_K), \tag{37}$$

$$\frac{5}{4\pi}C_2 = S_2^2\frac{8}{15}\epsilon \sim \mathcal{O}(\epsilon\Omega_K^2), \tag{38}$$

where we define the coefficients S_ℓ by

$$\begin{aligned}S_\ell &= \int_0^1 da(\sqrt{-K}(\eta_0 - \eta(a)))^\ell \frac{\partial}{\partial a} \\ &\quad \times \left(\frac{1}{F(a)}\int_0^a da' \frac{8\pi G\rho_{\rm DE}(a')F(a')}{3a'H^2(a')}\right),\end{aligned} \tag{39}$$

where we used $\rho_{\rm DE}(a) = m_0^2\varphi^2/2$. The approximate expression in the above formulas are obtained by $\sqrt{-K}\eta \sim \sqrt{-K}/H_0 \sim \sqrt{\Omega_K}$. We evaluate higher multipoles in a similar manner, which are approximately given by

$$C_\ell \sim \mathcal{O}(\epsilon\Omega_K^\ell). \tag{40}$$

These higher multipoles with $\ell \geq 3$ do not put tighter constraints compared with the dipole and the quadrupole as long as $\Omega_K \ll 1$. Thus, the dipole and the quadrupole are the most important, which is reflected by the property that the typical scales of the spatial variation are given by the supercurvature scale. Using the results for S_ℓ in Appendix E, numerical calculations of S_ℓ give the following results

$$S_1 \simeq 1.1 \times 10^{-1} \Omega_K^{1/2}, \tag{41}$$

$$S_2 \simeq 0.9 \times 10^{-1} \Omega_K, \tag{42}$$

where we assumed $\Omega_m = 0.3$ and $\Omega_K \ll 1$.

The observed values of the dipole and the quadrupole in the CMB anisotropies are found in the literature. The dipole of the CMB is approximately expressed as

$$\frac{\delta T_{\rm dipole}}{T} = \frac{v}{c} \cos\theta, \tag{43}$$

where v is the peculiar velocity of the observer and $\cos\theta$ is the parameter related to the line-of-sight. The raw observational result gives $v \approx 370$ km/s [37,38]. From this observation, we adopt the value of the dipole moment,

$$C_1^{\rm obs} \approx 6.3 \times 10^{-6}, \tag{44}$$

where we used $3C_1/4\pi = (v/c)^2$. Comparing this with (37) and (41), we have the constraint from the dipole

$$\epsilon \Omega_K \lesssim 4.9 \times 10^{-5}. \tag{45}$$

The measurement of C_2 from the Planck Legacy Archive obtained with Planck satellite [39] with 1σ error is

$$\frac{2 \times 3}{2\pi} C_2^{\rm obs} = 2.26^{+5.33}_{-1.32} \times \frac{10^2 \mu {\rm K}^2}{(2.725\ {\rm K})^2}. \tag{46}$$

If we adopt the upper bound of the above observed value, taking the effect of the observational error, we have

$$\frac{2 \times 3}{2\pi} C_2^{\rm obs} < 1.0 \times 10^{-10}. \tag{47}$$

Then, Eq. (47) with (38) and (42) leads to

$$\epsilon \Omega_K^2 < 1.0 \times 10^{-8}. \tag{48}$$

The constraints given by Eqs. (45) and (48) contain the parameter ϵ describing some properties of the ancestor vacuum Eq. (1) along with the curvature parameter Ω_K. The two parameters Ω_K and ϵ are coupled to each other in Eqs. (45) and (48), which are natural outcomes because this scenario connects the spatial curvature with the supercurvature-mode dark energy through the CDL tunneling inflation. Consequently, the constraint on the ancestor vacuum parameter ϵ is linked with the value of the spatial curvature Ω_K. The upper bound of the spatial curvature is given by $|\Omega_K| \lesssim 10^{-2}$–$10^{-3}$ [4], and if we take the possible value with BAO for $\Omega_K \sim 10^{-3}$, the other parameter is constrained to satisfy the relation $\epsilon \lesssim 10^{-2}$.

IV. CONCLUSIONS

We have studied a model of the dark energy in the universe created by a bubble nucleation due to quantum tunneling from an ancestor vacuum. The supercurvature mode of an ultralight scalar field ϕ in the bubble of the present universe plays a role of the dark energy, which we call the supercurvature-mode dark energy. In such a universe, the present universe is open and has a negative spatial curvature in the bubble and fluctuations of the supercurvature modes are frozen on the superhorizon scales. This is the reason that the mode behaves as the dark energy in the present epoch.

In the present paper, we have particularly investigated large-scale inhomogeneity of the supercurvature-mode dark energy density. We show that the density contrast of the dark energy becomes of the order of one on the supercurvature scale $L_{\rm sc}$, which is much longer than the Hubble length H_0^{-1} in the present universe; $L_{\rm sc} \gg H_0^{-1}$, and the spatial variation might be extremely tiny within H_0^{-1}. Nevertheless, our calculations indicate that the large-scale inhomogeneity of the dark energy density can be detected in the anisotropies of the CMB spectrum via the late-time ISW effect. The detectable signatures are imprinted at low angular momentum components of the two-point correlation function of the CMB temperature fluctuation, especially the dipole and the quadrupole. Comparing with the current observations of the CMB multipoles, we obtained upper bounds of the curvature parameter Ω_K and the ancestor vacuum parameter ϵ, given in Eqs. (45) and (48), respectively. For example, if we assume that the spatial curvature is given by the current upper limit from observations, $\Omega_K \sim 10^{-3}$, the other parameter is given by $\epsilon \lesssim 10^{-2}$. For a smaller value of Ω_K, ϵ can be larger. Further investigations of the supercurvature-mode dark energy scenario will be interesting in view of the large-scale CMB anomaly (e.g., [40–44]).

String theory predicts axionlike particles(ALPs) [21,22] which are ultralight. In an open inflation scenario created by a bubble nucleation of the true vacuum due to quantum tunneling from the false ancestor vacuum, the supercurvature-modes of these ultralight scalar fields provide a candidate for the dark energy.

The supercurvature-mode dark energy scenario predicts a deviation of the equation of state from the cosmological constant [24] as well as the spatial variation presented in the present paper. The universe also predicts negative spatial curvature. Hence the model could be potentially verified/falsified by future observations.

ACKNOWLEDGMENTS

This work was supported by the Ministry of Education, Culture, Sports, Science and Technology (MEXT)/Japan Society for the Promotion of Science (JSPS) KAKENHI Grants No. 15H05895, No. 16H03977, No. 17K05444, No. 17H06359 (K. Y.), No. 17K14304 (D. Y.), No. 16K05329, and No. 18H03708 (S. I.). We acknowledge Y. Sekino for collaboration at the early stage and also for critical comments. We also thank M. Sasaki for useful discussions.

APPENDIX A: CORRELATION FUNCTION OF THE SUPERCURVATURE MODE

First, we recall the correlation function of the scalar field ϕ in the CDL geometry, analytically continued to Lorentzian. For more details, see Ref. [24]. Taking only the contributions from the supercurvature modes with $k = i(1-\epsilon)$, it is given in Eq. (4.5) in [24] as

$$\langle\phi(\eta,R)\phi(\eta',0)\rangle^{(\mathrm{scm})} = \frac{-2\pi i}{8\pi^2 a(\eta)a(\eta')} \cdot \mathrm{Res}(i(1-\epsilon))\mathrm{e}^{(1-\epsilon)(\eta+\eta'+2\tilde{\eta}_1)} \times \frac{1}{\sin\epsilon\pi}\frac{\sinh(1-\epsilon)R}{\sinh R}, \tag{A1}$$

where $a(\eta)$ is the scale factor, and $\mathrm{Res}(i(1-\epsilon))$ denotes the residue of the reflection coefficient $\mathcal{R}(k)$ at the pole $k = i(1-\epsilon)$, whose explicit form is given in [24]. R is the radial coordinate parametrizing the spatial slice H^3. $\tilde{\eta}_1$ is a phase shift introduced for connecting the CDL and FLRW geometries smoothly, and can be expressed as

$$\mathrm{e}^{\tilde{\eta}_1} = \frac{H_A}{H_I}(1+\mathrm{e}^{2X_0}), \tag{A2}$$

where X_0 is related to the size of the bubble ($X_0 \to -\infty$ corresponds to a small bubble limit). For small ϵ, Eq. (A1) reduces to Eq. (2) with

$$\varphi(\eta) = c_*^{1/2}\frac{H_A^2}{m_A}\left(\frac{H_I}{H_A}\right)^{\epsilon}\varphi_*(\eta), \tag{A3}$$

where c_* is an $\mathcal{O}(1)$ constant (Eq. (5.33) in [24]). $\varphi_*(\eta)$ represents the time evolution in the FLRW universe, and, for instance, in the periods (ii) and (iii) in Sec. V C of Ref. [24], it is given by

$$\varphi_*(\eta) \simeq \frac{\sin m_0 t}{m_0 t}, \tag{A4}$$

where t is the proper time in the FLRW universe. When $m_0 \lesssim H_0$ is satisfied, $m_0 t \lesssim 1$, and we have $\varphi_*(\eta) \simeq 1$; the supercurvature mode is almost frozen.

With the frozen supercurvature modes, we can set e.g., $\eta = 0$. Then in the flat limit $\Omega_K \ll 1$, the supercurvature modes behave as the dark energy with the density

$$\frac{8\pi G}{3}\rho_{\mathrm{DE}} \simeq \frac{8\pi G}{3}\frac{m_0^2\varphi^2(0)}{2} = H_0^2\Omega_\Lambda. \tag{A5}$$

In the massless limit, $\epsilon \to 0$, and using a small bubble approximation $X_0 \to -\infty$, the well-known result for the coincident-point correlation function [45]

$$\langle\phi^2\rangle = \varphi^2(0) = \frac{3}{8\pi^2}\frac{H_A^4}{m_A^2} \tag{A6}$$

is reproduced.

APPENDIX B: EQUATION OF STATE OF DARK ENERGY

In the previous paper Ref. [25], the authors investigated the dynamical property of the supercurvature-mode dark energy and showed that the EoS is modified from $w = -1$. In this Appendix, we show that this modification gives a higher order correction to the large-scale spatial inhomogeneity and can be neglected in the present investigation, which justifies our approximation using $w = -1$.

As was pointed out in Eq. (3) in Ref. [25] and Eq. (5.59) in Ref. [24], the contributions from the time-derivative terms to the pressure p and the energy density ρ can be ignored in comparison with the spatial-derivative terms and mass terms as long as the conditions $m_0 \ll H_0$ and $\epsilon \ll 1$ are satisfied. Then, the evolution of EoS w of the supercurvature-mode dark energy yields

$$w(z) = \frac{p}{\rho} = -\frac{1+\frac{2}{3}\tilde{\epsilon}(1+z)^2}{1+2\tilde{\epsilon}(1+z)^2} = -1+\frac{\frac{4}{3}\tilde{\epsilon}(1+z)^2}{1+2\tilde{\epsilon}(1+z)^2}, \tag{B1}$$

where z is the cosmological redshift and $\tilde{\epsilon}$ is defined as

$$\tilde{\epsilon} \equiv \frac{1}{(m_0/H_0)^2}\epsilon\Omega_K \gtrsim \mathcal{O}(\epsilon\Omega_K), \tag{B2}$$

with $\Omega_K = 1/(H_0^2R_c^2)$. In the above approximate equality, we assumed $m_0 \lesssim H_0$; e.g., $10^{-1}H_0 \lesssim m_0 \lesssim H_0$. Then, under the condition of Eq. (45), $\tilde{\epsilon} \ll 1$ follows. If we define the present EoS and its derivative by $w_0 \equiv w(z=0)$ and $w_1 \equiv -a\frac{dw}{da}|_{a=1}$ in the Chevallier-Polarski-Linder (CPL) parametrization [46,47], Eq. (B1) gives the deviation of EoS w_0 from -1 as

$$w_0 + 1 = \frac{\frac{4}{3}\tilde{\epsilon}}{1+2\tilde{\epsilon}} \simeq \frac{4}{3}\tilde{\epsilon}, \tag{B3}$$

and its derivative as

$$w_1 = \frac{\frac{8}{3}\tilde{\epsilon}}{(1+2\tilde{\epsilon})^2} \simeq \frac{8}{3}\tilde{\epsilon} = 2(w_0+1). \tag{B4}$$

Equations (B3) and (B4) confirm that the deviation of dark energy EoS from $w=-1$ at late times before and at present epoch is small as long as $\tilde{\epsilon} \ll 1$ holds. The deviation from $w=-1$ gives a higher order correction to the investigation of large-scale inhomogeneity and can be neglected in the leading order calculations of the C_l's.

APPENDIX C: ONE-POINT PROBABILITY FUNCTION OF DARK ENERGY

In this Appendix, we demonstrate the explicit form of the probability functions of the dark energy density and the density parameter. For a *normalized* probability variable of the field, the distribution function is given by

$$P(\tilde{\phi}(\boldsymbol{x})) = \frac{1}{\sqrt{2\pi}} \exp\left[-\frac{1}{2}\tilde{\phi}^2(\boldsymbol{x})\right]. \tag{C1}$$

We note that $\langle \tilde{\phi}^2(\boldsymbol{x}) \rangle = 1$. Using $\tilde{\phi}(\boldsymbol{x})$, we may write the scalar field as $\phi(\eta,\boldsymbol{x}) = \varphi(\eta)\tilde{\phi}(\boldsymbol{x})$, where $\varphi(0)$ is defined in Appendix A. We find the probability density function of the supercurvature-mode dark energy density, given by

$$\rho_{\rm DE}(\boldsymbol{x}) = \frac{1}{2}m_0^2\phi^2(\eta_0,\boldsymbol{x}) \approx \frac{1}{2}m_0^2\varphi^2(0)\tilde{\phi}^2(\boldsymbol{x}). \tag{C2}$$

On the large scales $R > R_{\rm sc}$, the spatial variation is significant, however, as long as we consider a region of the present Hubble horizon, which is much smaller than the scale $R_{\rm sc}$, $\rho_{\rm DE}(\boldsymbol{x})$ can be regarded as a probability variable through $\tilde{\phi}$ by Eq. (C2). Following the conservation of the probability,

$$d\tilde{\phi}(\boldsymbol{x})P(\tilde{\phi}(\boldsymbol{x})) = d\rho_{\rm DE} f(\rho_{\rm DE}), \tag{C3}$$

we define the probability density function of $\rho_{\rm DE}(\boldsymbol{x})$

$$f(\rho_{\rm DE}) = \int d\tilde{\phi}(\boldsymbol{x})\delta(\rho_{\rm DE} - \rho_{\rm DE}(\boldsymbol{x}))P(\tilde{\phi}(\boldsymbol{x})). \tag{C4}$$

It can be analytically calculated as

$$f(\rho_{\rm DE}) = \frac{1}{\sqrt{4\pi m_0^2\varphi^2(0)}} \frac{\exp\left(-\rho_{\rm DE}/m_0^2\varphi^2(0)\right)}{\sqrt{\rho_{\rm DE}/m_0^2\varphi^2(0)}}, \tag{C5}$$

which is plotted in Fig. 4. This figure demonstrates a wide distribution of probability of $\rho_{\rm DE}$ at scales larger than the supercurvature scale $R_{\rm sc}$ even when we fix the parameter as Eq. (11).

We also discuss the probability density function of the dark energy density parameter defined by

$$\Omega_\Lambda(\boldsymbol{x}) = \frac{\rho_{\rm DE}(\boldsymbol{x})}{\rho_{\rm DE}(\boldsymbol{x}) + \rho_m} = \frac{\bar{\Omega}_\Lambda\tilde{\phi}^2(\boldsymbol{x})}{1-\bar{\Omega}_\Lambda + \bar{\Omega}_\Lambda\tilde{\phi}^2(\boldsymbol{x})}, \tag{C6}$$

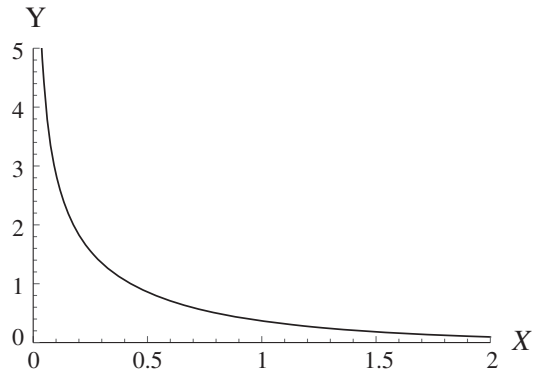

FIG. 4. Probability density function $f(\rho_{\rm DE})$ as a function of $\rho_{\rm DE}$. The horizontal axis is $X = \rho_{\rm DE}/m_0^2\varphi^2(0)$, and the vertical axis is $Y = \sqrt{4\pi}m_0^2\varphi^2(0)f(\rho_{\rm DE})$.

where ρ_m is the dark matter energy density. In a similar way to the case for the dark energy density, we can find the probability density function of Ω_Λ as

$$f(\Omega_\Lambda) = \int d\tilde{\phi}\delta(\Omega_\Lambda - \Omega_\Lambda(\boldsymbol{x}))P(\tilde{\phi}(\boldsymbol{x})). \tag{C7}$$

It can be analytically calculated as

$$f(\Omega_\Lambda) = \frac{1}{2\sqrt{2\pi}\Omega_\Lambda(1-\Omega_\Lambda)}\sqrt{\frac{\Omega_\Lambda(1-\bar{\Omega}_\Lambda)}{\bar{\Omega}_\Lambda(1-\Omega_\Lambda)}} \times \exp\left(-\frac{\Omega_\Lambda(1-\bar{\Omega}_\Lambda)}{2\bar{\Omega}_\Lambda(1-\Omega_\Lambda)}\right). \tag{C8}$$

Figure 5 plots the function $f(\Omega_\Lambda)$ assuming $\bar{\Omega}_\Lambda = 0.7$ in Eq. (C8). $f(\Omega_\Lambda)$ has a peak at a point of Ω_Λ slightly larger than $\bar{\Omega}_\Lambda = 0.7$, but this figure demonstrates a wide distribution of probability of Ω_Λ at scales larger than the supercurvature scale $R_{\rm sc}$.

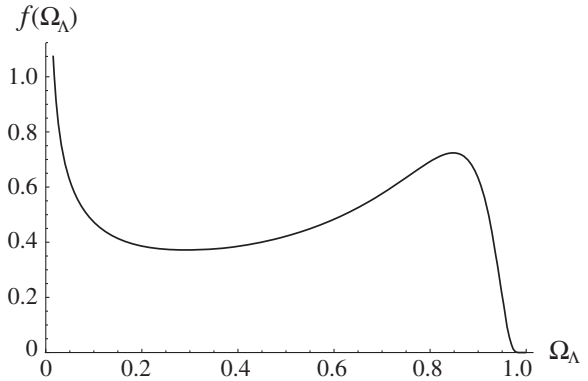

FIG. 5. Probability density function $f(\Omega_\Lambda)$ of Ω_Λ with its expectation value fixed as $\overline{\Omega_\Lambda} = 0.7$.

APPENDIX D: DERIVATION OF EQ. (35)

The expectation value in (34) can be decomposed into products of two-point functions by using the Wick-theorem in Eq. (7):

$$\langle(\phi^2(X)-\phi^2(0))(\phi^2(X')-\phi^2(0'))\rangle = 2(\langle\phi(X)\phi(X')\rangle^2 - \langle\phi(X)\phi(0')\rangle^2 - \langle\phi(0)\phi(X')\rangle^2 + \langle\phi(0)\phi(0')\rangle^2). \quad \text{(D1)}$$

Here, $X, X', 0, 0'$ denote $(\eta,\chi,\boldsymbol{\gamma})$, $(\eta',\chi',\boldsymbol{\gamma}')$, $(\eta,0,\gamma)$, and $(\eta',0,\gamma')$, respectively. Then, using the two-point correlation function given in Eq. (2), Eq. (D1) can be evaluated as

$$\begin{aligned}\langle(\phi^2(X)-\phi^2(0))(\phi^2(X')-\phi^2(0'))\rangle &= 2\varphi^2(\eta)\varphi^2(\eta')\left(\frac{\sinh^2(1-\epsilon)R}{(1-\epsilon)^2\sinh^2R} - \frac{\sinh^2(1-\epsilon)R_1}{(1-\epsilon)^2\sinh^2R_1} - \frac{\sinh^2(1-\epsilon)R_2}{(1-\epsilon)^2\sinh^2R_2} + 1\right)\\ &= -4\varphi^2(\eta)\varphi^2(\eta')(R\coth R - R_1\coth R_1 - R_2\coth R_2 + 1)\epsilon + \mathcal{O}(\epsilon^2)\\ &\simeq -4\varphi^2(\eta)\varphi^2(\eta')\left(\frac{1}{3}(R^2 - R_1^2 - R_2^2) + \frac{1}{45}(-R^4 + R_1^4 + R_2^4) + \mathcal{O}(R^6)\right)\epsilon, \end{aligned} \quad \text{(D2)}$$

where $R_i = \sqrt{-K}\chi_i$ for $i = 1, 2$. The schematic relation of R, R_1, and R_2 is presented in Fig. 1. In the expansion of $\coth(R_i)$, we used $R_1 = \sqrt{-K}\chi_1 \ll 1$ and $R_2 = \sqrt{-K}\chi_2 \ll 1$.

Using the relation of Eq. (3), we have

$$\begin{aligned}\frac{1}{3}(R^2 - R_1^2 - R_2^2) + \frac{1}{45}(-R^4 + R_1^4 + R_2^4) &\simeq -\frac{2}{3}R_1R_2\left(1 - \frac{2}{15}(R_1^2 + R_2^2)\right)\cos\psi - \frac{2}{15}R_1^2R_2^2\left(\frac{3}{2}\cos^2\psi - \frac{1}{2}\right)\\ &\simeq -\frac{2}{3}R_1R_2\cos\psi - \frac{2}{15}R_1^2R_2^2\left(\frac{3}{2}\cos^2\psi - \frac{1}{2}\right). \end{aligned} \quad \text{(D3)}$$

Substituting Eqs. (D2) and (D3) into Eq. (34), we obtain Eq. (35).

APPENDIX E: ESTIMATIONS OF S_ℓ

The conformal time η and scale factor a are related by

$$\frac{1}{a^2}\frac{da}{d\eta} = H(a), \quad \text{(E1)}$$

where the evolution of the Hubble parameter obeys the Friedmann equation. When the dark energy is approximated by the cosmological constant, we may express

$$H^2(a) = \frac{8\pi G}{3}(\rho_m + \rho_{\rm DE}) - \frac{K}{a^2} \equiv H_0^2\left(\frac{\Omega_m}{a^3} + \frac{\Omega_K}{a^2} + (1 - \Omega_m - \Omega_K)\right). \quad \text{(E2)}$$

We assume a nearly flat FLRW universe by adopting $\Omega_m \approx 0.3$, $\Omega_\Lambda \approx 0.7$, and $\Omega_K \approx 0$, and we approximate S_ℓ defined by Eq. (39) as

$$S_\ell = \int_0^1 da(\sqrt{-K}(\eta_0 - \eta(a)))^\ell \frac{\partial}{\partial a}\left(\frac{G(a)}{F(a)}\right), \quad \text{(E3)}$$

where

$$G(a) = \int_0^a da' \frac{8\pi G\rho_{\rm DE}(a')F(a')}{3a'H^2(a')} = \int_0^a da' \frac{(1-\Omega_m)a'^2F(a')}{\Omega_m + (1-\Omega_m)a'^3}, \quad \text{(E4)}$$

$$F(a) = F_c\exp\left\{\int_0^a \frac{da'}{a'}\left(1 + \frac{3\Omega_m}{2[\Omega_m + (1-\Omega_m)a'^3]}\right)\right\} \equiv \frac{F_c a^{5/2}}{\sqrt{\Omega_m + (1-\Omega_m)a^3}}. \quad \text{(E5)}$$

From Eq. (E1), the conformal time is written as

$$\eta(a) = \int_0^a \frac{da'}{a'^2 H(a')} = H_0^{-1} \int_0^a \frac{da'}{a'^2 (1 - \Omega_m + \Omega_m a'^{-3})^{1/2}}. \tag{E6}$$

An approximate expression for S_ℓ is given by substituting (E4), (E5) and (E6) into (E3). We evaluate numerically the integrations over a, and obtain Eqs. (41) and (42).

[1] P. A. R. Ade *et al.* (Planck Collaboration), Astron. Astrophys. **594**, A13 (2016).
[2] P. A. R. Ade *et al.* (Planck Collaboration), Astron. Astrophys. **594**, A14 (2016).
[3] P. A. R. Ade *et al.* (Planck Collaboration), Astron. Astrophys. **594**, A17 (2016).
[4] N. Aghanim *et al.* (Planck Collaboration), arXiv:1807.06209.
[5] D. H. Weinberg, M. J. Mortonson, D. J. Eisenstein, C. Hirata, A. G. Riess, and E. Rozo, Phys. Rep. **530**, 87 (2013).
[6] G. Obied, H. Ooguri, L. Spodyneiko, and C. Vafa, arXiv:1806.08362.
[7] P. Agrawal, G. Obied, P. J. Steinhardt, and C. Vafa, Phys. Lett. B **784**, 271 (2018).
[8] H. Ooguri, E. Palti, G. Shiu, and C. Vafa, Phys. Lett. B **788**, 180 (2019).
[9] S. K. Garg and C. Krishnan, arXiv:1807.05193.
[10] S. Appleby, R. Battye, and A. Moss, Phys. Rev. D **81**, 081301 (2010).
[11] A. Tripathia, A. Sangwana, and H. K. Jassala, J. Cosmol. Astropart. Phys. 06 (2017) 012.
[12] S. Vagnozzi, S. Dhawan, M. Gerbino, K. Freese, A. Goobar, and O. Mena, Phys. Rev. D **98**, 083501 (2018).
[13] S. Tsujikawa, Classical Quantum Gravity **30**, 214003 (2013).
[14] C. Ringeval, T. Suyama, T. Takahashi, M. Yamaguchi, and S. Yokoyama, Phys. Rev. Lett. **105**, 121301 (2010).
[15] D. Glavan, T. Prokopec, and V. Prymidis, Phys. Rev. D **89**, 024024 (2014).
[16] D. Glavan, T. Prokopec, and D. C. van der Woude, Phys. Rev. D **91**, 024014 (2015).
[17] D. Glavan, T. Prokopec, and T. Takahashi, Phys. Rev. D **94**, 084053 (2016).
[18] D. Glavan, T. Prokopec, and A. A. Starobinsky, Eur. Phys. J. C **78**, 371 (2018).
[19] H. Aoki, S. Iso, and Y. Sekino, Phys. Rev. D **89**, 103536 (2014).
[20] H. Aoki and S. Iso, Prog. Theor. Exp. Phys. **2015**, 113E02 (2015).
[21] A. Arvanitaki, S. Dimopoulos, S. Dubovsky, N. Kaloper, and J. March-Russell, Phys. Rev. D **81**, 123530 (2010).
[22] P. Svrcek and E. Witten, J. High Energy Phys. 06 (2006) 015.
[23] L. Visinelli and S. Vagnozzi, Phys. Rev. D **99**, 063517 (2019).
[24] H. Aoki, S. Iso, D.-S. Lee, Y. Sekino, and C.-P. Yeh, Phys. Rev. D **97**, 043517 (2018).
[25] D. Yamauchi, H. Aoki, S. Iso, D.-S. Lee, Y. Sekino, and C.-P. Yeh, arXiv:1807.07904.
[26] S. R. Coleman and F. De Luccia, Phys. Rev. D **21**, 3305 (1980).
[27] B. Freivogel, M. Kleban, M. R. Martinez, and L. Susskind, J. High Energy Phys. 03 (2006) 039.
[28] R. Bousso, D. Harlow, and L. Senatore, Phys. Rev. D **91**, 083527 (2015).
[29] B. Freivogel, M. Kleban, M. R. Martinez, and L. Susskind, arXiv:1404.2274.
[30] A. H. Guth and Y. Nomura, Phys. Rev. D **86**, 023534 (2012).
[31] M. Sasaki, T. Tanaka, and K. Yamamoto, Phys. Rev. D **51**, 2979 (1995).
[32] K. Yamamoto, M. Sasaki, and T. Tanaka, Phys. Rev. D **54**, 5031 (1996).
[33] J. Garriga, X. Montes, M. Sasaki, and T. Tanaka, Nucl. Phys. **B551**, 317 (1999).
[34] L. Amendola *et al.*, Living Rev. Relativity **21**, 2 (2018).
[35] A. H. Chamseddine and V. Mukhanov, J. Cosmol. Astropart. Phys. 02 (2016) 040.
[36] W. Hu, arXiv:astro-ph/9508126.
[37] P. J. E. Peebles, *Principles of Physical Cosmology* (Princeton University Press, Princeton, New Jersey, 1993).
[38] N. Aghanim *et al.* (Planck Collaboration), Astron. Astrophys. **571**, A27 (2014).
[39] N. Aghanim *et al.* (Planck Collaboration), arXiv:1807.06209.
[40] A. Rassat, J.-L. Starck, P. Paykari, F. Sureau, and J. Bobin, J. Cosmol. Astropart. Phys. 08 (2014) 006.
[41] H. K. Eriksen, A. J. Banday, K. M. Gorski, F. K. Hansen, and P. B. Lilje, Astrophys. J. **660**, L81 (2007).
[42] P. A. R. Ade *et al.* (Planck Collaboration), Astron. Astrophys. **594**, A16 (2016).
[43] D. J. Schwarz, C. J. Copi, D. Huterer, and G. D. Starkman, Classical Quantum Gravity **33**, 184001 (2016).
[44] S. Aiola, B. Wang, A. Kosowsky, T. Kahniashvili, and H. Firouzjahi, Phys. Rev. D **92**, 063008 (2015).
[45] A. Linde, *Particle physics and inflationary cosmology* (CRC press, Boca Raton, Florida, 1990).
[46] M. Chevallier and D. Polarski, Int. J. Mod. Phys. D **10**, 213 (2001).
[47] E. V. Linder, Phys. Rev. Lett. **90**, 091301 (2003).